# Platinum Nanoparticles Supported on Anatase Titanium Dioxide as Highly Active Catalysts for Aerobic Oxidation under Visible Light Irradiation

Yasuhiro Shiraishi,*,[†] Daijiro Tsukamoto,[†] Yoshitsune Sugano,[†] Akimitsu Shiro,[†] Satoshi Ichikawa,[‡] Shunsuke Tanaka,[§] and Takayuki Hirai[†]

[†]Research Center for Solar Energy Chemistry and Division of Chemical Engineering, Graduate School of Engineering Science, Osaka University, Toyonaka 560-8531, Japan

[‡]Institute for NanoScience Design, Osaka University, Toyonaka 560-8531, Japan

[§]Department of Chemical, Energy and Environmental Engineering, Kansai University, Suita 564-8680, Japan

**S** *Supporting Information*

**ABSTRACT:** Visible light irradiation ($\lambda$ >450 nm) of platinum (Pt) nanoparticles supported on anatase titanium dioxide ($TiO_2$) promotes efficient aerobic oxidation at room temperature. This occurs via the electronic excitation of Pt particles by visible light followed by the transfer of their electrons to anatase conduction band. The positively charged Pt particles oxidize substrates, whereas the conduction band electrons are consumed by the reduction of molecular oxygen. The activity of this photocatalysis depends on the height of Schottky barrier and the number of perimeter Pt atoms created at the Pt/anatase heterojunction, which are affected by the amount of Pt loaded and the size of Pt particles. The catalyst loaded with 2 wt % Pt, containing 3−4 nm Pt particles, creates a relatively low Schottky barrier and a relatively large number of perimeter Pt atoms and, hence, facilitates smooth Pt→anatase electron transfer, resulting in very high photocatalytic activity. This catalyst is successfully activated by sunlight and enables efficient and selective aerobic oxidation of alcohols at ambient temperature.

**KEYWORDS:** photocatalysis, platinum nanoparticles, anatase titanium dioxide, visible light, aerobic oxidation
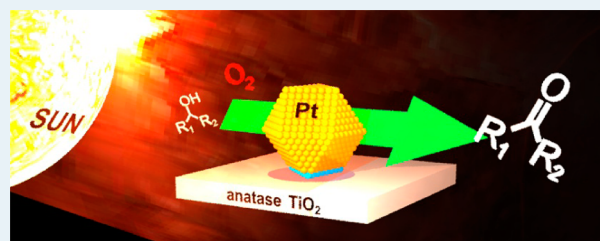
## INTRODUCTION

Aerobic oxidation by heterogeneous catalysts with molecular oxygen ($O_2$) as an oxidant is an essential process for the synthesis of various chemicals.[1] Photocatalytic oxidation with $O_2$ has also been studied extensively with semiconductor materials such as titanium dioxide ($TiO_2$);[2−6] several types of substrates such as alcohols, amines, hydrocarbons, and sulfides are successfully oxidized at atmospheric pressure and room temperature. One of the critical issues for practical application of photocatalytic processes is the low catalytic activity under irradiation of visible light ($\lambda$ >400 nm), the main component of solar irradiance. Several $TiO_2$ materials doped with nitrogen,[7,8] sulfur,[9,10] carbon,[11,12] or boron atoms[13] have been proposed to extend the absorption edge of catalysts into the visible region. These doped catalysts, however, suffer from low quantum yields for reaction (<0.5%), because they inherently contain a large number of crystalline lattices that act as charge recombination centers.[14] Development of visible-light-driven catalysts that promote highly efficient aerobic oxidation is still a challenge.

Nanosized noble metals such as gold (Au) and silver (Ag) absorb light in the visible region because of a resonant oscillation of free electrons coupled by light, known as localized surface plasmon resonance (SPR).[15] Application potentiality of SPR to photocatalysis was first discovered by Tian et al.[16] Visible light irradiation of Au particles loaded on a $TiO_2$ film that is coated on an indium tin oxide electrode generates an anodic photocurrent in the presence of $Fe^{2+}$. This occurs via a collective oscillation of electrons ($e^-$) on the Au particles induced by visible light and a subsequent transfer of $e^-$ to the $TiO_2$ conduction band. Simultaneously, the positively charged Au particles receive $e^-$ from the electron donor ($Fe^{2+}$). This suggests that visible light irradiation successfully creates the charge-transferred state at the metal/semiconductor hetero-junction and would promote catalytic oxidation and reduction reactions, that is, plasmonic photocatalysis.[17,18]

Very recently, we found that visible-light-induced plasmonic photocatalysis successfully promotes aerobic oxidation of alcohols at the Au/semiconductor interface.[19] This is achieved by Au particles loaded on a mixture of anatase/rutile $TiO_2$ (Degussa, P25). The activity of Au/P25 catalyst critically depends on its architecture; Au particles with about 4 nm
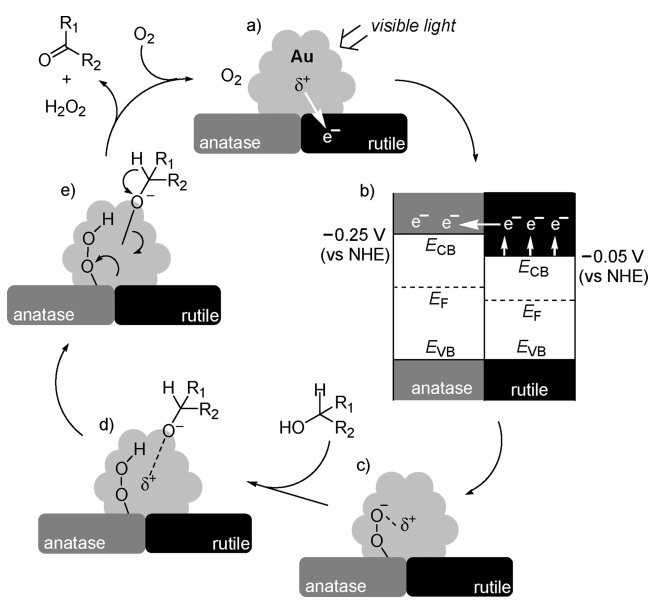
diameter located at the interface of anatase/rutile $TiO_2$ are necessary. The plasmonic reaction on Au/P25 proceeds via the multistep $e^-$ transfer, as summarized in Scheme 1. The

**Scheme 1. Aerobic Oxidation of Alcohol on the Au/P25 Catalyst Activated by Visible Light**



photoactivated Au particles transfer $e^-$ to rutile (a). The $e^-$ is then transferred to the adjacent anatase (b). $O_2$ is reduced on the anatase surface by $e^-$ and produces a peroxo-type oxygen anion ($O-O^-$) (c). Alcohol is adsorbed onto the positively charged Au particles via the interaction of its H atom with the $O-O^-$ species, producing an Au–alcoholate species (d).[20] Subsequent removal of H atom from the species produces the corresponding aldehydes or ketones (e). The apparent quantum yield for this reaction is 3.8% by the irradiation of 550 nm monochromatic light, which is much higher than that obtained with the doped photocatalysts (<0.5%).[7−13] The metal/semiconductor system is chemically stable under aerated condition as compared to the doped photocatalysts.[17] The plasmonic photocatalysis therefore has a potential for visible-light-induced aerobic oxidation.

The next challenge is further activity improvement of the plasmonic photocatalysts. In the plasmonic reaction, the charge separation is facilitated by the reduction of $O_2$ on the semiconductor surface with the $e^-$ transferred from the photoactivated metal particles. The anatase surface is active for $O_2$ reduction, whereas rutile surface is inactive.[21] In contrast, photoactivated Au particles scarcely transfer $e^-$ to anatase, probably because of the weak Au/anatase interaction, but the $e^-$ transfer to rutile does occur.[19] Therefore, as shown in Scheme 1, the Au/P25 system requires the Au→rutile→anatase multistep $e^-$ transfers for reaction. This circuitous process may suppress smooth $e^-$ transfer and decrease the reaction efficiency. In particular, the rutile→anatase $e^-$ transfer (Scheme 1b) is probably the rate-determining step. This is because the conduction band potential ($E_{CB}$) of rutile is more positive than $E_{CB}$ of anatase, and the rutile→anatase $e^-$ transfer requires a negative shift of rutile $E_{CB}$ by the accumulation of $e^-$ on its conduction band.[22,23] Development of more efficient plasmonic photocatalysts therefore requires the creation of

metal/anatase heterojunction that enables direct $e^-$ transfer to anatase.

Pt particles also exhibit an absorption band in the visible region, which is assigned to the intraband transition of electrons from the sp band to the sp-conduction band (SPR absorption) and the interband transition of electrons from d band to sp-conduction band.[24] The intensity of this absorption is much weaker than that of Au particles.[15] There is only one report of photocatalysis driven by visible light activation of Pt particles; Zhai et al.[25] reported that Pt particles loaded on a $TiO_2$ thin film promote dehydrogenation of alcohols by visible light ($\lambda$ >420 nm) under $N_2$ atmosphere. Herein, we report that Pt particles with 3−4 nm diameter loaded on anatase $TiO_2$, when used for aerobic oxidation under visible light, facilitate direct $e^-$ transfer to anatase and promote the reaction highly efficiently. The Pt/anatase catalysts promote aerobic oxidation of alcohols with an apparent quantum yield 7.1% (550 nm), which is much higher than that obtained with the Au/P25 catalyst (3.8%).[19] In addition, the catalyst successfully promotes the reaction even under irradiation of sunlight.

## ■ RESULTS AND DISCUSSION

**Preparation and Properties of Catalysts.** The Pt/$TiO_2$ catalysts were prepared by impregnation of Pt precursors followed by reduction with $H_2$,[26,27] using anatase (Japan Reference Catalyst, JRC-TIO-1; average particle size, 21 nm; Brunauer−Emmett−Teller (BET) surface area, 81 $m^2$ $g^{-1}$), P25 (JRC-TIO-4; 24 nm; 57 $m^2$ $g^{-1}$; anatase/rutile = ca. 83/17), and rutile $TiO_2$ particles (JRC-TIO-6; 15 nm; 104 $m^2$ $g^{-1}$), supplied by the Catalyst Society of Japan. $TiO_2$ was added to water containing $H_2PtCl_6$, and the water was removed by evaporation with vigorous stirring. The resultant was calcined in air for 2 h and reduced with $H_2$ for 2 h at the identical temperature, affording $Pt_{x(y)}$/$TiO_2$ as brown powder. The $x$ is the amount of Pt loaded [$x$ (wt %) = Pt/(Pt + $TiO_2$) × 100], and $y$ is the temperature (K) for calcination and reduction treatments.

As shown in Figure 1a, the transmission electron microscopy (TEM) images of $Pt_{2(673)}$/anatase catalysts exhibit mono-dispersed Pt particles; the average diameter of particles ($d_{Pt}$) is 3.4 nm. In addition, the high-resolution TEM images of catalysts (Figure 1b) reveal that the Pt particles can be indexed as *fcc* structures, as is the case for bulk Pt (JCPDS 04-0802). $Pt_{2(673)}$/P25 and $Pt_{2(673)}$/rutile also contain Pt particles with similar $d_{Pt}$ (3.1 and 2.9 nm; Supporting Information, Figure S1). X-ray photoelectron spectroscopy (XPS) of the catalysts shows distinctive Pt 4f peaks at 71 and 74 eV (Supporting Information, Figure S2), indicating that Pt atoms exist as metallic state.[28] As shown in Figure 2a, diffuse reflectance UV−vis spectra of the catalysts containing 2 wt % Pt exhibit broad absorption band at $\lambda$ >400 nm, assigned to the intraband and interband transitions of Pt particles.[29] Their absorption intensities are much lower than those of Au particles on the $Au_2$/P25 catalyst containing 2 wt % Au.[19]

**Catalytic Activity.** The activity of Pt/$TiO_2$ catalysts was studied by oxidation of benzyl alcohol (**1**) to benzaldehyde (**2**), a typical aerobic oxidation.[30] The reactions were performed by stirring a toluene solution (5 mL) containing **1** (0.1 mmol) and catalyst (5 mg) under $O_2$ atmosphere (1 atm). The temperature of solution was kept rigorously at 298 ± 0.5 K. Figure 3 summarizes the amount of **2** produced by 12 h reaction in the dark (black bars) or visible light irradiation by a Xe lamp ($\lambda$ >450 nm, white bars). It is noted that both

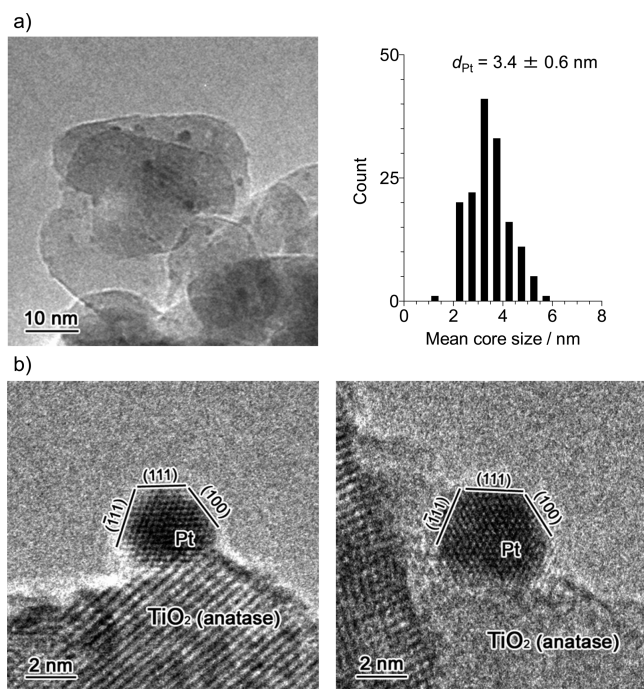a)



b)

**Figure 1.** (a) TEM image of $Pt_{2(673)}$/anatase catalyst and size distribution of the Pt particles. (b) High-resolution TEM images.



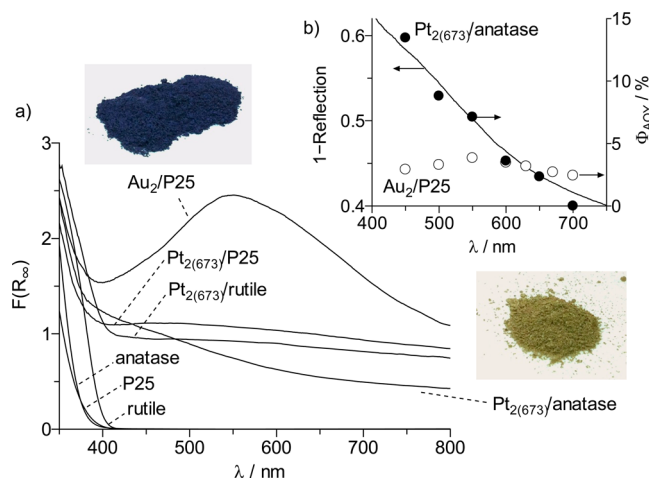**Figure 2.** (a) Diffuse reflectance UV−vis spectra of catalysts. (b) Action spectra for photocatalytic oxidation of **1** on (black) $Pt_{2(673)}$/anatase and (white) $Au_2$/P25 catalysts. The apparent quantum yield for the **2** formation was calculated with the following equation: $\Phi_{AQY}$ (%) = $[\{(Y_{vis} - Y_{dark}) \times 2\}/(\text{photon number entered into the reaction vessel})] \times 100$, where $Y_{vis}$ and $Y_{dark}$ are the amounts of **2** formed ($\mu$mol) under light irradiation and dark conditions, respectively.

reactions selectively produced **2** (mass balance: >99%). With bare anatase $TiO_2$, almost no reaction occurred in the dark, and visible light irradiation produced only 2 $\mu$mol of **2**. In contrast, the dark reaction with $Pt_{2(673)}$/anatase produced 12 $\mu$mol of **2** because of the high catalytic activity of Pt particles for aerobic oxidation.[31−33] Light irradiation further enhanced the reaction; twice the amount of **2** (25 $\mu$mol) was produced. This suggests that visible light irradiation of Pt/anatase catalyst indeed enhances aerobic oxidation.[34] It is noted that the activity of Pt/anatase catalyst is much higher than that of $Au_2$/P25 catalyst;[19] $Au_2$/P25 produced only 7.8 $\mu$mol of **2** even under photo-irradiation. Zhai et al.[25] reported that Pt/$TiO_2$ catalyst
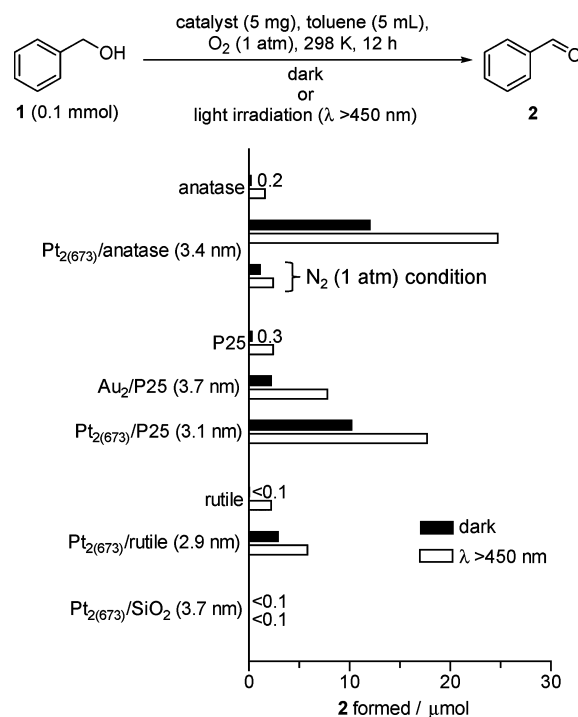


**Figure 3.** Amount of **2** formed during aerobic oxidation of **1** with respective catalysts, (black) in the dark or (white) visible light irradiation ($\lambda$ >450 nm; light intensity at 450−800 nm, 16.8 mW cm$^{-2}$). The data obtained under $N_2$ (1 atm) condition were also shown in the figure. Average diameter of metal particles on the catalysts is denoted in the parentheses. The detection limit of **2** is 0.02 $\mu$mol (4 $\mu$M), and the range of calibration is 0.004−20 mM.

promotes oxidation of alcohols by visible light ($\lambda$ >420 nm) under $N_2$ atmosphere; however, as shown in Figure 3, photoirradiation of $Pt_{2(673)}$/anatase under $N_2$ produced very small amount of aldehyde. This indicates that aerobic oxidation is much more efficient for alcohol oxidation.

Semiconductor support is necessary for the reaction enhancement by visible light irradiation. As shown in Figure 3, $Pt_{2(673)}$/$SiO_2$ catalyst with $SiO_2$ support (Aldrich; average particle size, 16 nm; BET surface area, 625 m$^2$ g$^{-1}$) shows almost no reaction enhancement even by photoirradiation. Visible light irradiation of $Pt_{2(673)}$/P25 also enhances the reaction, but the enhancement is lower than that of $Pt_{2(673)}$/anatase. In addition, $Pt_{2(673)}$/rutile is almost inactive for reaction. As shown in Supporting Information, Figure S3, other anatase $TiO_2$ loaded with Pt particles also enhance aerobic oxidation under visible light irradiation. These data clearly suggest that Pt particles loaded on anatase $TiO_2$ promote efficient aerobic oxidation under visible light. As shown in Supporting Information, Figure S4, the Pt/anatase catalyst maintains its activity even after prolonged photo-irradiation (~36 h), indicating that the catalyst is stable under photoirradiation.

**Electron Transfer at the Pt/anatase Heterojunction.** The enhanced aerobic oxidation on the Pt/anatase catalyst under visible light is initiated by the intraband or interband transition of Pt particles. Some literatures[35,36] reported that Pt/$TiO_2$ promotes photocatalytic reaction under visible light ($\lambda$ >400 nm), although $TiO_2$ itself scarcely absorbs light at this wavelength range. This was explained by the narrowed bandgap of $TiO_2$ by the Pt loadings. In the present case, as shown in Figure 2b, the action spectrum analysis revealed that the

absorption band of $Pt_{2(673)}$/anatase correlates well with the apparent quantum yield ($\Phi_{AQY}$) for photocatalytic oxidation of **1** (black circle). This data clearly suggests that the enhanced aerobic oxidation on the Pt/anatase catalyst is triggered by the activation of Pt particles. It is also noted that $\Phi_{AQY}$ for $Pt_{2(673)}$/anatase is higher than that for $Au_2$/P25 (white circle)[19] at the broad wavelength range of incident light, especially at $\lambda < 600$ nm. The $\Phi_{AQY}$ values for $Pt_{2(673)}$/anatase at 450 and 550 nm are 13.7% and 7.1%, respectively, which are much higher than those for $Au_2$/P25 (2.9% and 3.8%).

In the Pt/anatase system, photoactivated Pt particles transfer $e^-$ to anatase, and the $e^-$ reduces $O_2$ on its surface. This is confirmed by electron spin resonance (ESR) analysis of the catalysts at 77 K, after treatment of the sample with $O_2$ at room temperature in the dark or visible light irradiation ($\lambda > 450$ nm). As shown in Figure 4a (blue), bare anatase $TiO_2$ treated with
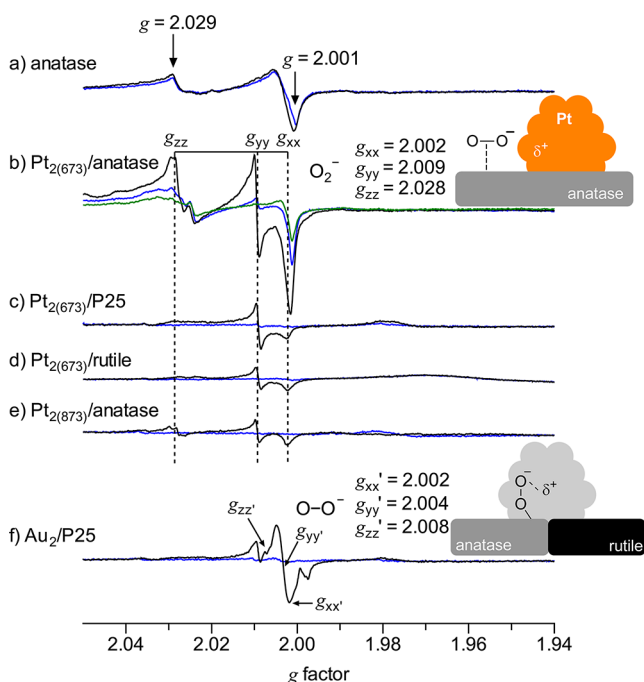


**Figure 4.** ESR spectra of respective catalysts. The catalysts were treated with 20 Torr $O_2$, (blue) in the dark at 298 K, (black) under visible light irradiation at 298 K, or (green) in the dark at 353 K. After evacuation, the samples were measured at 77 K.

$O_2$ in the dark shows weak signals ($g = 2.029, 2.001$), which are assigned to $O^-$ formed via a dissociative adsorption of $O_2$ onto the oxygen vacancy sites of $TiO_2$ surface.[37,38] Photoirradiation of this sample does not create any new signal (Figure 4a, black). As shown in Figure 4b, $Pt_{2(673)}$/anatase treated with $O_2$ in the dark also shows $O^-$ signal, but photoirradiation creates strong signals assigned to a superoxide-type oxygen anion ($O_2^-$; $g_{xx} = 2.002$, $g_{yy} = 2.009$, $g_{zz} = 2.028$), which is stabilized on the $TiO_2$ surface.[39] This suggests that photoactivated Pt particles indeed transfer $e^-$ to anatase and promote the reduction of $O_2$ on its surface. As shown in Figure 4c and d, photoirradiation of $Pt_{2(673)}$/P25 and $Pt_{2(673)}$/rutile samples creates much weaker $O_2^-$ signals. This means that the $O_2$ reduction does not occur efficiently on these catalysts, and the data agree with their photocatalytic activities (Figure 3). It is noted that, as shown in Figure 4b (green), the Pt/anatase catalyst, when treated with $O_2$ at high temperature (353 K) in the dark, does not create an

$O_2^-$ signal. This indicates that photothermal conversion[40] on the Pt particles, even if it occurs in the present system,[41−44] does not promote $O_2$ reduction. This again suggests that electronic excitation of Pt particles by visible light enables $e^-$ transfer to anatase and promotes $O_2$ reduction.

In the Au/P25 system,[19] photoactivated Au particles scarcely transfer $e^-$ to anatase. However, in the Pt/anatase system, the Pt→anatase $e^-$ transfer occurs successfully. This is probably due to the strong affinity between Pt particles and anatase surface. Gong et al.[45] studied the adsorption properties of Pt and Au clusters onto the anatase (101) surface by means of scanning tunneling microscopy and ab initio calculations. They clarified that Pt clusters are strongly adsorbed onto the anatase surface via the association with the steps, terraces, and oxygen vacancy sites, and the adsorption energy for Pt/anatase is 10-fold higher than that for Au/anatase. The strong Pt/anatase interaction, therefore, probably enables the Pt→anatase $e^-$ transfer.

As shown in Figure 4b, photoirradiation of $Pt_{2(673)}$/anatase with $O_2$ produces superoxide-type oxygen anion ($O_2^-$). In contrast, $Au_2$/P25[19] (Figure 4f) generates peroxide-type oxygen anion ($O−O^-$; $g_{xx}' = 2.002$, $g_{yy}' = 2.004$, $g_{zz}' = 2.008$), associated with the residual positive charge on Au particles.[46] The formation of $O_2^-$ species on Pt/anatase is explained by the high $e^-$ diffusivity in the anatase conduction band. Sun et al.[47] reported that the $e^-$ diffusivity in anatase is 2-fold higher than that in rutile. This may allow smooth $e^-$ diffusion in anatase and promote $O_2$ reduction at the surface spatially separated from the Pt particles (Figure 4b). In contrast, on Au/P25, the Au→rutile→anatase multistep $e^-$ transfers (Scheme 1) suppress smooth $e^-$ diffusion and promote $O_2$ reduction at the surface near to the Au particles. This thus produces $O−O^-$ species associated with the residual positive charge on Au particles (Figure 4f).

The mechanism for photocatalytic reaction on Pt/anatase can be depicted as in Scheme 2B, similar to the mechanism in the dark (Scheme 2A). It is considered that the dark reaction is initiated by activation of $O_2$ on the anionic site of metal particles.[20] The activated species removes H atom of alcohol and produces hydroperoxide and alcoholate species on the Pt surface.[48] Subsequent removal of H atom from the species affords the product. In the photocatalytic reaction (Scheme 2B), photoactivated Pt particles transfer $e^-$ to anatase (a). The $e^-$ reduces $O_2$ and produces $O_2^-$ species (b). The $O_2^-$ species attracts H atom of alcohol and produces the hydroperoxide and alcoholate species (c). These species give rise to the product (d). These mechanisms suggest that both dark and photocatalytic reactions are initiated by the activation of $O_2$, leading to the formation of hydroperoxide and alcoholate species. Although it is unclear whether the dark and photocatalytic reactions affect each other, the $O_2$ reduction on anatase surface promoted by $e^-$ transfer from photoactivated Pt particles is the crucial step facilitating efficient aerobic oxidation.

**Effect of Pt Amount.** Photocatalytic activity of Pt/anatase catalysts depends on the amount of Pt loaded. This is confirmed by the reaction using $Pt_{x(673)}$/anatase catalysts with different Pt loadings $[x$ (wt %) = Pt/(Pt + $TiO_2$) × 100]. As shown in Figure 5a (orange), $d_{Pt}$ of the catalysts are similar (3.3−3.4 nm). In contrast, as shown in Figure 6a, absorbance of the catalysts in the visible region increases with the Pt loadings because of the increase in the number of Pt particles. The bar graphs in Figure 5a show the results for aerobic oxidation of **1** obtained with respective catalysts. The dark activity (black bar)

**Scheme 2. Proposed Mechanism for Aerobic Oxidation of Alcohol on the Pt/anatase Catalyst under (A) Dark and (B) Visible Light Irradiation Conditions**
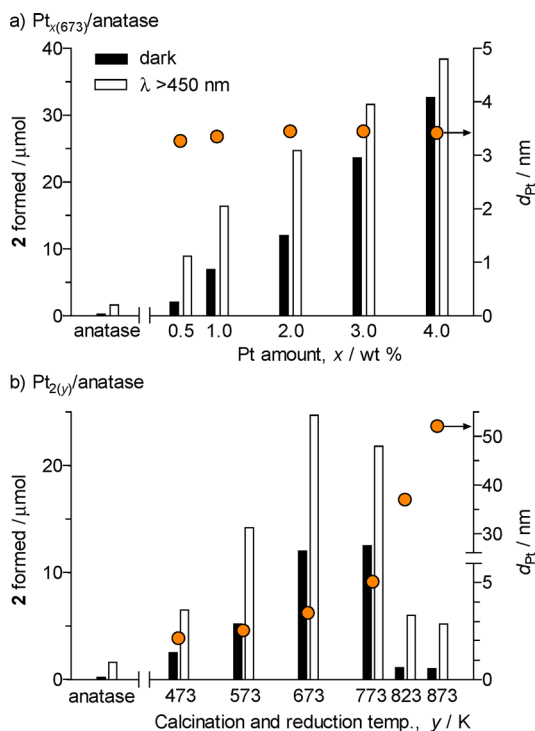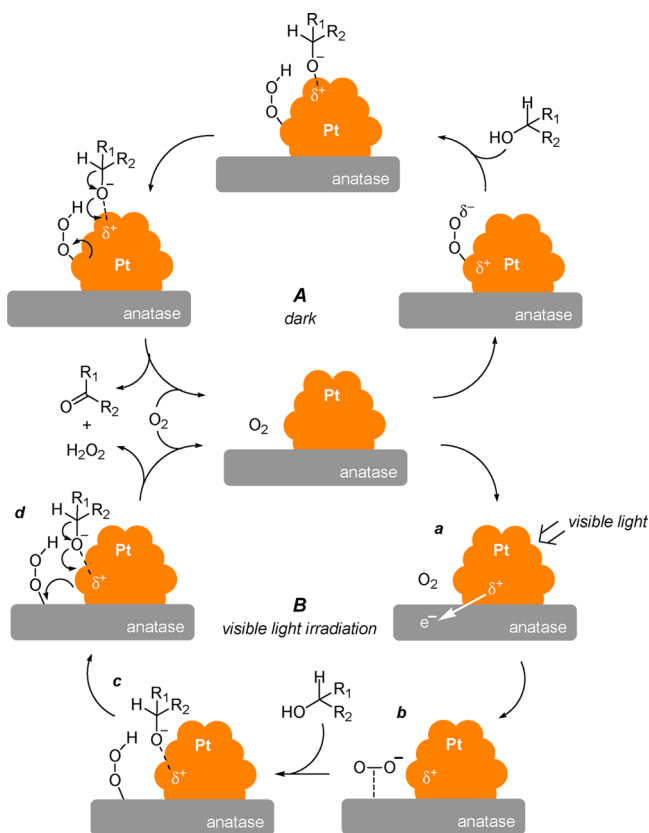




**Figure 5.** Amount of **2** formed during aerobic oxidation of **1** with (a) $Pt_{x(673)}$/anatase and (b) $Pt_{2(y)}$/anatase catalysts in the dark or under visible light irradiation. Orange keys denote $d_{Pt}$ of catalysts. The reaction conditions are identical to those in Figure 3.
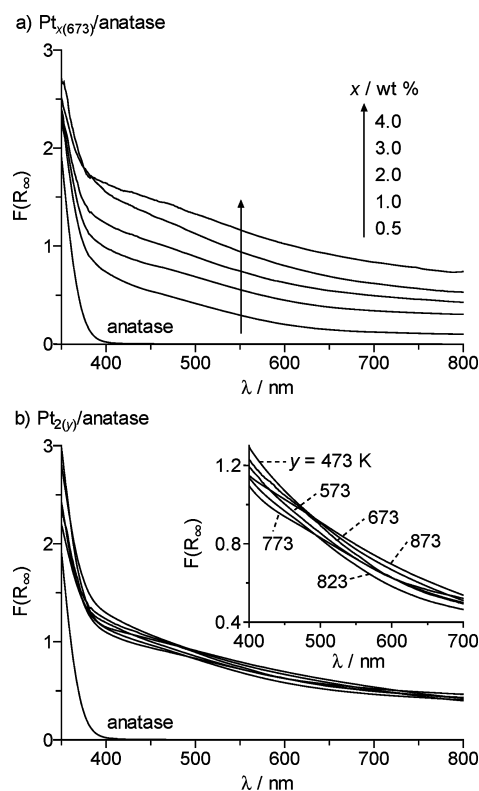


**Figure 6.** Diffuse reflectance UV–vis spectra of (a) $Pt_{x(673)}$/anatase and (b) $Pt_{2(y)}$/anatase catalysts.

increases with the Pt loadings because of the increase in the number of surface Pt atoms that are active for aerobic oxidation.[30] Visible light irradiation (white bar) further enhances the reaction, but the enhancement depends on the Pt loadings; 2 wt % Pt shows the largest enhancement, and higher loading catalysts are ineffective despite their stronger absorbance. As schematically shown in Scheme 3, the metal/semiconductor heterojunction creates a Schottky barrier ($\phi_B$).[49] Visible light irradiation leads to a collective oscillation of sp band or d band electrons on the metal particles and promotes the intraband or interband excitation to the sp-

**Scheme 3. Proposed Mechanism for Electron Transfer from the Photoactivated Pt Particles to Anatase**[a]
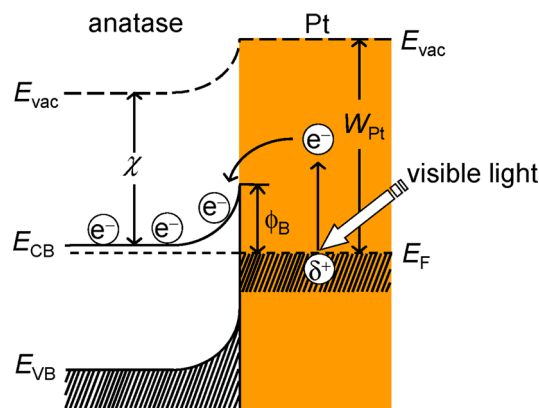


[a]$E_{vac}$, $E_F$, $W_{Pt}$, $\phi_B$, and $\chi$ denote the vacuum level, Fermi level, work function of Pt, Schottky barrier height ($= W_{Pt} - \chi$), and electron affinity of anatase conduction band, respectively.

conduction band. This provides energy to the electrons to overcome $\phi_B$ and facilitates e$^-$ transfer to the semiconductor conduction band.[50,51] The height of $\phi_B$, therefore, strongly affects the e$^-$ transfer efficiency. As reported,[52] the increase in the amount of metal loaded onto the semiconductor leads to an increase in $\phi_B$, because of the decrease in the Fermi level of the semiconductor. The decreased photocatalytic activity for larger Pt loading catalysts (Figure 5a) is therefore probably because the increased $\phi_B$ suppresses e$^-$ transfer from photoactivated Pt particles to anatase.

**Effect of Pt Particle Size.** The size of Pt particles also affects the photocatalytic activity. To clarify this, the Pt$_{2(y)}$/anatase catalysts with 2 wt % Pt were prepared at different calcination and reduction temperature, $y$ (K). As shown in Figure 5b (orange), $d_{Pt}$ of the catalysts increase with the temperature increase because of the sintering of Pt particles; $d_{Pt}$ for Pt$_{2(473)}$, Pt$_{2(573)}$, Pt$_{2(673)}$, Pt$_{2(773)}$, Pt$_{2(823)}$, and Pt$_{2(873)}$ catalysts are 2.1, 2.5, 3.4, 5.0, 39.1, and 52.8 nm, respectively. X-ray diffraction patterns of the catalysts indicate that the anatase-to-rutile phase transition scarcely occurs (Supporting Information, Figure S5). As shown by the black bars in Figure 5b, in the dark condition, the Pt$_{2(673)}$ catalyst shows the highest activity, and the catalysts with smaller or larger Pt particles show decreased activity. The low activity of smaller Pt particles is due to the decreased density of low-coordination Pt sites that are active for oxidation.[53] In contrast, larger Pt particles contain decreased number of surface Pt atoms and, hence, show decreased activity.[30]

As shown by the white bars in Figure 5b, the photocatalytic activity of Pt$_{2(y)}$/anatase shows $d_{Pt}$ dependence similar to the dark activity. The Pt$_{2(673)}$ catalyst shows the highest activity, and the catalysts with smaller or larger Pt particles show decreased activity. As shown in Figure 6b, absorbance of the catalysts in the visible region is similar, although their $d_{Pt}$ are different (Figure 5b). This indicates that the light absorption efficiencies for these catalysts are similar. The low photocatalytic activity of the catalysts with smaller Pt particles is due to the higher $\phi_B$ created at the Pt/anatase heterojunction. As reported,[54] the work function of metal particles ($W_M$) increases with a decrease in their particle size and is expressed by the following equation:

$$W_M(\text{eV}) = W_{M\infty} + \frac{1.08}{d_M} \qquad (1)$$

$W_{M\infty}$ and $d_M$ are the work function of planar metal and the diameter of metal particles, respectively. $W_{Pt\infty}$ is 5.65 eV,[55] and $W_{Pt}$ for Pt particles on the Pt$_{2(473)}$, Pt$_{2(573)}$, Pt$_{2(673)}$, Pt$_{2(773)}$, Pt$_{2(823)}$, and Pt$_{2(873)}$ catalysts are determined using their $d_{Pt}$ values to be 6.16, 6.08, 5.97, 5.87, 5.68, and 5.67 eV, respectively. As summarized in Figure 7 (black), $W_{Pt}$ for Pt particles indeed becomes more positive with a decrease in the particle size. As shown in Scheme 3, $\phi_B$ is defined as the difference between the work function of Pt particles and the electron affinity of anatase $E_{CB}$ ($\phi_B = W_{Pt} - \chi$).[56] This suggests that the catalysts with smaller Pt particles create higher $\phi_B$. This may suppress smooth e$^-$ transfer from the photoactivated Pt particles to anatase, resulting in lower photocatalytic activity (Figure 5b).

In contrast, larger Pt particles create lower $\phi_B$ because of their lower $W_{Pt}$; therefore, the e$^-$ transfer to anatase would occur more easily. However, as shown in Figure 5b, photocatalytic activity of the catalysts with larger Pt particles is much lower than that of Pt$_{2(673)}$. As shown in Scheme 4, the
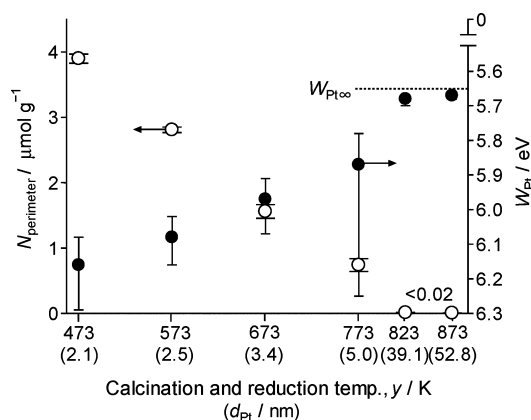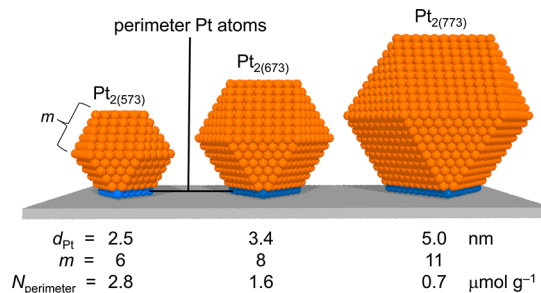


**Figure 7.** Work function of Pt particles ($W_{Pt}$) and the number of perimeter Pt atoms ($N_{perimeter}$) for Pt$_{2(y)}$/anatase catalysts, determined with the eqs 1−5 using $d_{Pt}$ values. The detailed calculation results are shown in Supporting Information, Table S1.

**Scheme 4. Relationship between the Pt Particle Size and the Number of Perimeter Pt Atoms for Pt$_{2(y)}$/anatase**[a]



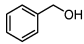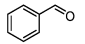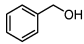[a]The calculation details for $N_{perimeter}$ are summarized in Supporting Information, Table S1.

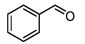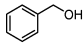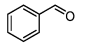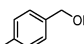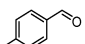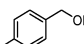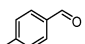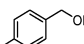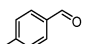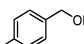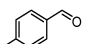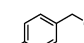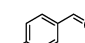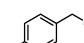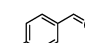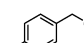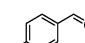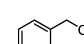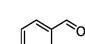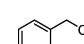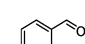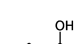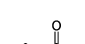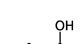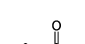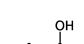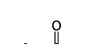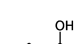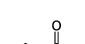e$^-$ transfer from photoactivated Pt particles to anatase occurs through the perimeter Pt atoms indicated by the blue spheres and, hence, the number of perimeter Pt atoms may affect the e$^-$ transfer efficiency. As shown in Figure 1b, the high-resolution TEM images of catalysts revealed that the shape of Pt particles is a part of a cuboctahedron, which is surrounded by (111) and (100) surfaces. The Pt particles on the anatase surface therefore can simply be modeled as a *fcc* cuboctahedron,[57] as often used for related systems.[58,59] This thus allows rough determination of the number of perimeter Pt atoms. Considering the full shell close packing cuboctahedron for Pt particle where one Pt atom is surrounded by twelve others, the number of total Pt atoms per particle ($N_{total}$*) can be expressed by eq 2 using the number of shells ($m$). $N_{total}$* is rewritten with the average diameter of Pt particle ($d_{Pt}$) and the atomic diameter of Pt [$d_{atom,Pt}$ (=0.278 nm)].[60] The number of perimeter Pt atoms per particle ($N_{perimeter}$*) is expressed by eq 3.[57]

$$N_{total}*(-) = \frac{10m^3 - 15m^2 + 11m - 3}{3}$$

$$= \left( \frac{d_{Pt}}{1.105 \times d_{atom,Pt}} \right)^3 \qquad (2)$$

$$N_{perimeter}*(-) = 3m - 3 \qquad (3)$$

The number of Pt particles per gram catalyst ($N_{particle}$) is expressed by eq 4, using the percent amount of Pt loaded onto

**Table 1. Effect of Sunlight Exposure on Aerobic Oxidation of Alcohols with Pt and Au Catalysts[a]**

| entry | substrate | catalyst | sunlight[b] | conversion / %[c] | product | yield / %[d] |
|---|---|---|---|---|---|---|
| 1 | (benzyl alcohol) | Pt$_{2(673)}$/anatase | + | 75 | (benzaldehyde) | 72 |
| 2 |  | Pt$_{2(673)}$/anatase | − | 13 |  | 12 |
| 3 |  | Au$_2$/P25 | + | 37 |  | 35 |
| 4 | (4-methylbenzyl alcohol) | Pt$_{2(673)}$/anatase | + | 84 | (4-methylbenzaldehyde) | 80 |
| 5 |  | Pt$_{2(673)}$/anatase | − | 9 |  | 9 |
| 6 |  | Au$_2$/P25 | + | 60 |  | 59 |
| 7 | (4-methoxybenzyl alcohol, MeO) | Pt$_{2(673)}$/anatase | + | >99 | (4-methoxybenzaldehyde, MeO) | 99 |
| 8 |  | Pt$_{2(673)}$/anatase | − | 14 |  | 14 |
| 9 |  | Au$_2$/P25 | + | 77 |  | 77 |
| 10 | (4-chlorobenzyl alcohol, Cl) | Pt$_{2(673)}$/anatase | + | 73 | (4-chlorobenzaldehyde, Cl) | 73 |
| 11 |  | Pt$_{2(673)}$/anatase | − | 7 |  | 7 |
| 12 |  | Au$_2$/P25 | + | 43 |  | 40 |
| 13 | (1-phenylethanol) | Pt$_{2(673)}$/anatase | + | 72 | (acetophenone) | 72 |
| 14 |  | Pt$_{2(673)}$/anatase | − | 11 |  | 10 |
| 15 |  | Au$_2$/P25 | + | 34 |  | 34 |
| 16 | (4-methoxy-1-phenylethanol, MeO) | Pt$_{2(673)}$/anatase | + | 85 | (4-methoxyacetophenone, MeO) | 84 |
| 17 |  | Pt$_{2(673)}$/anatase | − | 5 |  | 5 |
| 18 |  | Au$_2$/P25 | + | 49 |  | 49 |

[a]Reaction conditions: toluene (5 mL), alcohol (25 $\mu$mol), catalyst (5 mg), O$_2$ (1 atm), exposure time (4 h). The average light intensity at 300−800 nm was 8.1 mW cm$^{-2}$, which involves $\lambda$ <400 nm light with only about 2%. The solution temperature during exposure was 288−293 K. [b]The dark reaction (−) was performed at 293 K. [c]= (alcohol converted)/(initial amount of alcohol) × 100. [d]= (product formed)/(initial amount of alcohol) × 100.

the catalyst [$x$ (= 2 wt %)], molecular weight of Pt [$M_W$ (= 195.1 g mol$^{-1}$)], and $N_{total}$*. The number of perimeter Pt atoms per gram catalyst ($N_{perimeter}$) is therefore expressed by eq 5.

$$N_{particle}(\text{mol g}^{-1}) = \frac{x}{100 \times M_W \times N_{total}*} \quad (4)$$

$$N_{perimeter}(\text{mol g}^{-1}) = N_{perimeter}* \times N_{particle} \quad (5)$$

The $N_{perimeter}$ values for respective Pt$_{2(y)}$/anatase catalysts can therefore be calculated using their $d_{Pt}$ determined by the TEM observations (Supporting Information, Table S1). As shown in Figure 7 (white), the $N_{perimeter}$ values decrease with an increase in the Pt particle size; the value for Pt$_{2(473)}$ is 3.9 $\mu$mol g$^{-1}$, but that for Pt$_{2(873)}$ is only 6.9 × 10$^{-3}$ $\mu$mol g$^{-1}$. This suggests that the particle size increase leads to significant decrease in $N_{perimeter}$. As shown in Figure 3e, ESR analysis of the Pt$_{2(873)}$ catalyst after treatment with O$_2$ under visible light irradiation shows an O$_2^-$ signal much weaker than that of Pt$_{2(673)}$ (Figure 3b). This indicates that the catalysts with larger Pt particles are indeed inefficient for e$^-$ transfer to anatase, although their $\phi_B$ values are lower. These findings clearly suggest that the decreased number of perimeter Pt atoms suppresses e$^-$ transfer from photoactivated Pt particles to anatase and results in lower photocatalytic activity. As shown in Figure 5b, the Pt$_{2(573)}$, Pt$_{2(673)}$, and Pt$_{2(773)}$ catalysts contain Pt particles with similar sizes (2−5 nm), but the Pt$_{2(673)}$ catalyst shows the highest photocatalytic activity. This means that, as shown in Figure 7, the Pt particle size strongly affects W$_{Pt}$ and $N_{perimeter}$, and this trade-off relationship is critical for the activity of photocatalysis. As summarized in Scheme 4, the 3−4 nm Pt particles with shell number 7−10, create relatively low $\phi_B$ and relatively large number of perimeter Pt atoms at the Pt/anatase heterojunction and, hence, act as highly active photocatalysts.

The Pt$_{2(673)}$/anatase catalyst successfully promotes aerobic oxidation of alcohols under sunlight irradiation at ambient temperature. Table 1 summarizes the results for oxidation of

various alcohols obtained with Pt$_{2(673)}$/anatase catalyst under sunlight exposure, where the temperature of solution during reaction was 288−293 K. Sunlight exposure selectively oxidizes alcohols to the corresponding carbonyl compounds with very high yields (72−99%). These yields are much higher than those obtained with Pt$_{2(673)}$/anatase in the dark at 293 K or with the Au$_2$/P25 catalyst[19] under sunlight exposure. These data suggest that the Pt/anatase catalyst is successfully activated by sunlight and acts as efficient photocatalyst.

## ■ CONCLUSION

We found that Pt nanoparticles loaded on anatase TiO$_2$ behave as highly efficient photocatalysts driven by visible light irradiation. The high photocatalytic activity of this system is due to the smooth e$^-$ transfer from photoactivated Pt particles to anatase. This promotes efficient O$_2$ reduction on the anatase surface and facilitates charge separation at the Pt/anatase interface. The activity of this photocatalysis depends on the height of Schottky barrier and the number of perimeter Pt atoms. The catalyst with 2 wt % Pt, containing 3−4 nm Pt nanoparticles, facilitates efficient e$^-$ transfer from the photo-activated Pt particles to anatase and shows the highest photocatalytic activity. Sunlight activation of the catalyst successfully promotes selective and efficient oxidation of alcohols. The efficient charge separation at the Pt/anatase heterojunction clarified here may contribute to the development of more active catalysts and the design of photocatalytic systems for selective organic transformations by sunlight.

## ■ EXPERIMENTAL SECTION

**Preparation of Catalysts.** Pt$_{x(y)}$/TiO$_2$ catalysts [$x$ (wt %) = 0.5, 1, 2, 3, 4; $y$ (K) = 473, 573, 673, 773, 823, 873] were prepared as follows. TiO$_2$ (1.0 g) was added to water (20 mL) containing H$_2$PtCl$_6$·6H$_2$O (13.3, 26.8, 54.2, 82.1, or 110.6 mg). The solvents were removed by evaporation at 353 K with vigorous stirring. The obtained powders were calcined under air

flow and then reduced under $H_2$ flow at the identical temperature ($y$). The heating rate was 2 K min$^{-1}$ and the holding time at the designated temperature was 2 h, respectively. $Pt_{2(673)}/SiO_2$ was prepared in a similar manner.

$Au_2$/P25 was prepared by the deposition-precipitation method as described previously.[19] P25 $TiO_2$ (1.0 g) was added to water (50 mL) containing $HAuCl_4 \cdot 4H_2O$ (45.8 mg). The pH of solution was adjusted to about 7 with 1 mM NaOH, and the solution was stirred at 353 K for 3 h. The particles were recovered by centrifugation, washed with water, and dried at 353 K for 12 h. The powders were calcined under air flow, where the heating rate was 2 K min$^{-1}$ and the holding time at 673 K was 2 h.

**Reaction Procedure.** Catalyst (5 mg) was added to toluene (5 mL) containing an alcohol within a Pyrex glass tube ($\varphi$ 10 mm; capacity, 20 mL), and the tube was sealed with a rubber septum cap. The catalyst was dispersed well by ultrasonication for 5 min, and $O_2$ was bubbled through the solution for 5 min. The tube was immersed in a temperature-controlled water bath (298 ± 0.5 K)[61] and photoirradiated at $\lambda$ >450 nm with magnetic stirring using a 2 kW Xe lamp (USHIO Inc.),[62] filtered through a CS3-72 glass (Kopp Glass Inc.). The light intensity at 450−800 nm was 16.8 mW cm$^{-2}$. Sunlight reactions were performed on January 30, 2012 at 10:00−14:00 at the top of the laboratory building (north latitude 34.7°, east longitude 135.5°). The light intensity at 300−800 nm was 8.1 mW cm$^{-2}$ (Supporting Information, Figure S6). The highest temperature of solution during the sunlight exposure was 293 K, and the dark experiments were carried out at 293 K. After the reactions, the catalyst was recovered by centrifugation, and the solution was subjected to GC-FID analysis, where the concentrations of substrates and products were calibrated with authentic samples.

**Action Spectrum Analysis.** The photoreactions were carried out in a toluene solution (2 mL) containing **1** (0.4 mmol) with $Pt_{2(673)}$/anatase or $Au_2$/P25 catalyst (8 mg) using a Pyrex glass tube. After ultrasonication and $O_2$ bubbling, the tube was photoirradiated using a 2 kW Xe lamp, where the incident light was monochromated by band-pass glass filters (Asahi Techno Glass Co.). The full-width at half-maximum (fwhm) of the light was 11−16 nm. The photon number entered into the reaction vessel was determined with a spectroradiometer USR-40 (USHIO Inc.).

**ESR Measurement.** The measurements were carried out at the X-band using a Bruker EMX-10/12 spectrometer with a 100 kHz magnetic field modulation at a microwave power level of 10.0 mW.[63] The magnetic field was calibrated using 1,1′-diphenyl-2-picrylhydrazyl (DPPH) as standard. Catalyst (20 mg) was placed in a quartz ESR tube, and the tube was evacuated at 423 K for 3 h and cooled to room temperature. $O_2$ (20 Torr) was introduced to the tube and kept for 10 min. The tube was photoirradiated at 298 K using a Xe lamp at $\lambda$ >450 nm. The tube was then evacuated for 10 min to remove the excess amount of $O_2$ and analyzed at 77 K.

**Analysis.** The total amount of Pt in the catalysts was analyzed by an inductively coupled argon plasma atomic emission spectrometer (ICAP-AES; SII Nanotechnology, SPS 7800), after dissolution of catalysts in an aqua regia. TEM observations were carried out using an FEI Tecnai G2 20ST analytical electron microscope operated at 200 kV. XPS analysis was performed using a JEOL JPS-9000MX spectrometer with Mg K$\alpha$ radiation as the energy source. Diffuse reflectance UV−vis spectra were measured on an UV−vis spectrophotometer

(Jasco Corp.; V-550 with Integrated Sphere Apparatus ISV-469) with $BaSO_4$ as a reference.[64]

## ASSOCIATED CONTENT

**ⓢ Supporting Information**

Calculation details (Table S1), TEM images and size distributions of Pt particles (Figure S1), XPS charts for catalysts (Figure S2), reaction data for other Pt/anatase catalysts (Figure S3), time-dependent change for product (Figure S4), XRD patterns of catalysts (Figure S5), spectral irradiance of light sources (Figure S6). This material is available free of charge via the Internet at http://pubs.acs.org.

## AUTHOR INFORMATION

**Corresponding Author**
*E-mail: shiraish@cheng.es.osaka-u.ac.jp.

**Notes**
The authors declare no competing financial interest.

## REFERENCES

(1) Sheldon, R. A.; Arends, I. W. C. E.; Dijksman, A. *Catal. Today* **2000**, *57*, 157−166.
(2) Fox, M. A.; Dulay, M. T. *Chem. Rev.* **1993**, *93*, 341−357.
(3) Maldotti, A.; Molinari, A.; Amadelli, R. *Chem. Rev.* **2002**, *102*, 3811−3836.
(4) Palmisano, G.; Augugliaro, V.; Pagliaro, M.; Palmisano, L. *Chem. Commun.* **2007**, 3425−3437.
(5) Fagnoni, M.; Dondi, D.; Ravelli, D.; Albini, A. *Chem. Rev.* **2007**, *107*, 2725−2756.
(6) Shiraishi, Y.; Hirai, T. *J. Photochem. Photobiol. C* **2008**, *9*, 157−170.
(7) Asahi, R.; Morikawa, T.; Ohwaki, T.; Aoki, K.; Taga, Y. *Science* **2001**, *293*, 269−271.
(8) Miyauchi, M.; Ikezawa, A.; Tobimatsu, H.; Irie, H.; Hashimoto, K. *Phys. Chem. Chem. Phys.* **2004**, *6*, 865−870.
(9) Ohno, T.; Akiyoshi, M.; Umebayashi, T.; Asai, K.; Mitsui, T.; Matsumura, M. *Appl. Catal., A* **2004**, *265*, 115−121.
(10) Yan, X.; Ohno, T.; Nishijima, K.; Abe, R.; Ohtani, B. *Chem. Phys. Lett.* **2006**, *429*, 606−610.
(11) Sakthivel, S.; Kisch, H. *Angew. Chem., Int. Ed.* **2003**, *42*, 4908−4911.
(12) Irie, H.; Watanabe, Y.; Hashimoto, K. *Chem. Lett.* **2003**, *32*, 772−773.
(13) Zhao, W.; Ma, W.; Chen, C.; Zhao, J.; Shuai, Z. *J. Am. Chem. Soc.* **2004**, *126*, 4782−4783.
(14) Chen, X.; Mao., S. S. *Chem. Rev.* **2007**, *107*, 2891−2959.
(15) Jain, P. K.; Huang, X.; El-Sayed, I. H.; El-Sayed, M. A. *Acc. Chem. Res.* **2008**, *41*, 1578−1586.
(16) Tian, Y.; Tatsuma, T. *J. Am. Chem. Soc.* **2005**, *127*, 7632−7637.
(17) Primo, A.; Corma, A.; García, H. *Phys. Chem. Chem. Phys.* **2011**, *13*, 886−910.
(18) Linic, S.; Christopher, P.; Ingram, D. B. *Nat. Mater.* **2011**, *10*, 911−921.
(19) Tsukamoto, D.; Shiraishi, Y.; Sugano, Y.; Ichikawa, S.; Tanaka, S.; Hirai, T. *J. Am. Chem. Soc.* **2012**, *134*, 6309−6315.
(20) Ishida, T.; Nagaoka, M.; Akita, T.; Haruta, M. *Chem.—Eur. J.* **2008**, *14*, 8456−8460.
(21) Ohno, T.; Sarukawa, K.; Matsumura, M. *J. Phys. Chem. B* **2001**, *105*, 2417−2420.
(22) Dunn, W. W.; Aikawa, Y.; Bard, A. J. *J. Am. Chem. Soc.* **1981**, *103*, 3456−3459.

(23) Fujii, M.; Kawai, T.; Kawai, S. *Chem. Phys. Lett.* **1984**, *106*, 517–522.

(24) Hao, Q.; Juluri, B. K.; Zheng, Y. B.; Wang, B.; Chiang, I.-K.; Jensen, L.; Crespi, V.; Eklund, P. C.; Huang, T. J. *J. Phys. Chem. C* **2010**, *114*, 18059–18066.

(25) Zhai, W.; Xue, S.; Zhu, A.; Luo, Y.; Tian, Y. *ChemCatChem* **2011**, *3*, 127–130.

(26) Shiraishi, Y.; Ikeda, M.; Tsukamoto, D.; Tanaka, S.; Hirai, T. *Chem. Commun.* **2011**, *47*, 4811–4813.

(27) Shiraishi, Y.; Takeda, Y.; Sugano, Y.; Ichikawa, S.; Tanaka, S.; Hirai, T. *Chem. Commun.* **2011**, *47*, 7863–7865.

(28) Silvestre-Albero, J.; Sepúlveda-Escribano, A.; Rodríguez-Reinoso, F.; Anderson, J. A. *J. Catal.* **2004**, *223*, 179–190.

(29) Bigall, N. C.; Härtling, T.; Klose, M.; Simon, P.; Eng, L. M.; Eychmüller, A. *Nano Lett.* **2008**, *8*, 4588–4592.

(30) Abad, A.; Corma, A.; García, H. *Chem.—Eur. J.* **2008**, *14*, 212–222.

(31) Proch, S.; Herrmannsdörfer, J.; Kempe, R.; Kern, C.; Jess, A.; Seyfarth, L.; Senker, J. *Chem.—Eur. J.* **2008**, *14*, 8204–8212.

(32) Ng, Y. H.; Ikeda, S.; Harada, T.; Morita, Y.; Matsumura, M. *Chem. Commun.* **2008**, 3181–3183.

(33) Hong, H.; Hu, L.; Li, M.; Zheng, J.; Sun, X.; Lu, X.; Cao, X.; Lu, J.; Gu, H. *Chem.—Eur. J.* **2011**, *17*, 8726–8730.

(34) The amount of **2** formed is proportional to the intensity of incident light. Photoreaction of **1** was performed with different light intensity by changing the distance from the light source to the samples. The amount of **2** formed by 12 h photoirradiation was 25 $\mu$mol (16.8 mW cm$^{-2}$), 35 $\mu$mol (38.0 mW cm$^{-2}$), and 45 $\mu$mol (54.9 mW cm$^{-2}$), respectively.

(35) Sun, B.; Smirniotis, P. G.; Boolchand, P. *Langmuir* **2005**, *21*, 11397–11403.

(36) Chen, H.-W.; Ku, Y.; Kuo, Y.-L. *Water Res.* **2007**, *41*, 2069–2078.

(37) Fenoglio, I.; Greco, G.; Livraghi, S.; Fubini, B. *Chem.—Eur. J.* **2009**, *15*, 4614–4621.

(38) Coronado, J. M.; Soria, J. *Catal. Today* **2007**, *123*, 37–41.

(39) Anpo, M.; Che, M.; Fubini, B.; Garrone, E.; Giamello, E.; Paganini, M. C. *Top. Catal.* **1999**, *8*, 189–198.

(40) Chen, X.; Zhu, H.-Y.; Zhao, J.-C.; Zheng, Z.-F.; Gao, X.-P. *Angew. Chem., Int. Ed.* **2008**, *47*, 5353–5356.

(41) Photothermal conversion on the photoirradiated Pt particles scarcely occurs in the present system. The temperature increase on the surface of an individual Pt particle in solution under photoirradiation can roughly be estimated by the equation, $\Delta T = \sigma_{abs} I/(4\pi R_{eq} \beta \kappa)$, where $\sigma_{abs}$ = absorption cross section, $I$ = intensity of the incident light, $R_{eq}$ = radius of a sphere with the same volume as the particle, $\beta$ = thermal capacitance coefficient dependent on nanoparticle aspect ratio, $\kappa$ = thermal conductivity of solvent (ref 42). The $\sigma_{abs}$ value for <100 nm Pt particles is reported to be $<1 \times 10^{-14}$ m$^2$ (ref 43). Other parameters for our catalysts are: $R_{eq}$ <30 nm, $I$ = 168 W m$^{-2}$, $\beta$ = 1, $\kappa$ = 0.13 W m$^{-1}$ K$^{-1}$ (ref 44). The theoretical temperature increase, $\Delta T$, is determined with these parameters to be $3.4 \times 10^{-5}$ K. This very small temperature increase suggests that photothermal conversion scarcely occur in the present Pt/anatase system.

(42) Baffou, G.; Quidant, R.; Abajo, F. J. G. *ACS Nano* **2010**, *4*, 709–716.

(43) Langhammer, C.; Kasemo, B.; Zorić, I. *J. Chem. Phys.* **2007**, *126*, 194702–194711.

(44) Zhang, Z.; Gu, H.; Fujii, M. *Exp. Therm. Fluid Sci.* **2007**, *31*, 593–599.

(45) Gong, X.-Q.; Selloni, A.; Dulub, O.; Jacobson, P.; Diebold, U. *J. Am. Chem. Soc.* **2008**, *130*, 370–381.

(46) Chowdhury, B.; Bravo-Suárez, J. J.; Mimura, N.; Lu, J.; Bando, K. K.; Tsubota, S.; Haruta, M. *J. Phys. Chem. B* **2006**, *110*, 22995–22999.

(47) Sun, B.; Vorontsov, A. V.; Smirniotis, P. G. *Langmuir* **2003**, *19*, 3151–3156.

(48) Fukuto, J. M.; Di Stefano, E. W.; Burstyn, J. N.; Valentine, J. S.; Cho, A. K. *Biochemistry* **1985**, *24*, 4161–4167.

(49) Schottky, W. *Z. Phys.* **1939**, *113*, 367–414.

(50) Furube, A.; Du, L.; Hara, K.; Katoh, R.; Tachiya, M. *J. Am. Chem. Soc.* **2007**, *129*, 14852–14853.

(51) Nishijima, Y.; Ueno, K.; Yokota, Y.; Murakoshi, K.; Misawa, H. *J. Phys. Chem. Lett.* **2010**, *1*, 2031–2036.

(52) Uchihara, T.; Matsumura, M.; Yamamoto, A.; Tsubomura, H. *J. Phys. Chem.* **1989**, *93*, 5870–5874.

(53) Liu, Y.; Tsunoyama, H.; Akita, T.; Xie, S.; Tsukuda, T. *ACS Catal.* **2011**, *1*, 2–6.

(54) Wood, D. M. *Phys. Rev. Lett.* **1981**, *46*, 749–759.

(55) Eastman, D. E. *Phys. Rev. B* **1970**, *2*, 1–2.

(56) Nakato, Y.; Ueda, K.; Yano, H.; Tsubomura, H. *J. Phys. Chem.* **1988**, *92*, 2316–2324.

(57) Benfield, R. E. *J. Chem. Soc. Faraday Trans.* **1992**, *88*, 1107–1110.

(58) Arruda, T. M.; Shyam, B.; Ziegelbauer, J. M.; Mukerjee, S.; Ramaker, D. E. *J. Phys. Chem. C* **2008**, *112*, 18087–18097.

(59) Wilson, O. M.; Knecht, M. R.; Garcia-Martinez, J. C.; Crooks, R. M. *J. Am. Chem. Soc.* **2006**, *128*, 4510–4511.

(60) Murthi, V. S.; Urian, R. C.; Mukerjee, S. *J. Phys. Chem. B* **2004**, *108*, 11011–11023.

(61) Tsukamoto, D.; Shiro, A.; Shiraishi, Y.; Sugano, Y.; Ichikawa, S.; Tanaka, S.; Hirai, T. *ACS Catal.* **2012**, *2*, 599–603.

(62) Shiraishi, Y.; Sugano, Y.; Tanaka, S.; Hirai, T. *Angew. Chem., Int. Ed.* **2010**, *49*, 1656–1660.

(63) Shiraishi, Y.; Saito, N.; Hirai, T. *J. Am. Chem. Soc.* **2005**, *127*, 8304–8306.

(64) Shiraishi, Y.; Saito, N.; Hirai, T. *J. Am. Chem. Soc.* **2005**, *127*, 12820–12822.